APPLICABILITY OF VARIOUS Pb-FREE SOLDER JOINT ACCELERATION FACTOR MODELS

Ron Zhang
Sun Microsystems
Sunnyvale, CA, USA

Jean-Paul Clech
EPSI Inc.
Montclair, NJ, USA

ABSTRACT
Pb-free solder joint acceleration factor (AF) models are of interest to the electronics industry for the simple reason that, combined with test failure data, they provide a quick way to assess solder interconnect reliability. Accurate values of AFs are needed to extrapolate test results to field conditions, thus allowing for an upfront estimate of board-level reliability. In this paper, an analytical approach is first used to calculate AFs from standard temperature cycling to field conditions on different Pb-free packages and board assemblies. The results are then compared with several Pb-free AF models as well as actual test data. AF predictions are compared for algebraic, compact and finite-element based models. Conclusions are drawn as to the accuracy of Pb-free AF models and conditions under which particular models are applicable.

Key words: Pb-free, SAC, Acceleration Factor, Solder Joint Reliability, Compact Strain Energy Model, Finite Element Model

INTRODUCTION

As part of a larger effort to quantify Pb-free solder joint reliability, this paper presents case studies comparing AFs between different models and several sets of accelerated test results. Accelerated thermal cycling is of use to precipitate potential failure modes and generate failure time distributions in a reduced amount of time. The projection of failure cycles to field conditions requires acceleration factors that are computed with an adequate level of accuracy. A variety of AFs or life prediction models have been proposed for solder joint reliability of Sn-Ag-Cu (SAC) assemblies, a partial review of which was given in [1]. All AFs come with errors, the bounds of which are rarely spelled out. AF models also have their limitations in terms of conditions over which they apply. It is thus important to assess both the accuracy and the applicability of AF models. This is a daunting task for any new technology, including Pb-free assembly technology.

AF MODELS

Three types of SAC reliability models were selected, representing the three grand classes of models that are commonly used for solder joint reliability assessment: an algebraic model; a one-dimensional or Compact Strain Energy (CSE) model that generates hysteresis loops for solder joints stresses and strains arising from global and local mismatches in Coefficients of Thermal Expansion (CTEs); and last, a three-dimensional Finite Element (FE) based model that can capture complex geometric details. All three models were developed for SAC Pb-free assemblies with SAC387/396 alloy composition. A brief description of each model is given hereafter.

Algebraic Model (AM)

The AM model [2] represents a first attempt at fitting a Norris-Landzberg [3] type of equation to accelerated thermal cycling results for SAC assemblies. The AF between test (subscript "t") and operating (subscript "o") conditions is given as:

$$AF \equiv \frac{N_o}{N_t} = \left(\frac{\Delta T_t}{\Delta T_o}\right)^{2.65} \left(\frac{t_t}{t_o}\right)^{0.136} \exp\left[2185\left(\frac{1}{T_{\max,\,o}} - \frac{1}{T_{\max,\,t}}\right)\right] \quad (1)$$

where, the AF is defined as the ratio of cycles to failure under operating and test conditions, ΔT's are temperature swings, t's are dwell times (presumably equal dwell times on the hot and cold sides of a cycle) and T_{max}'s (in Kelvin) are maximum temperatures. The three constants in the AF equation were obtained by fitting the model to failure times from 14 test cells in a design-of-experiment covering different component types (Ceramic BGA, CSP and TSOPs), temperature extremes (0/60ºC, 0/100ºC, 40/100ºC and -25/125ºC) and dwell times (10, 60 and 350 minutes). Characteristic lives covered one and three-quarter orders of magnitude in test lives, from 167 to 9455 cycles (9455/167 = 56 = $10^{1.75}$). Errors for predicted vs. measured AFs were estimated in the range of -25% to +50%. In a study of the applicability of the model, the authors [2] found that AF errors may increase when the model is applied to test conditions with cold temperatures of -40ºC or -55ºC, possibly due to a change in failure mechanism. Future changes in the model constants were also suggested [2] as additional test data becomes available for SAC assemblies.

Compact Strain Energy Model (CSEM)

This is a one-dimensional model where cyclic strain energy is given by the area of stabilized hysteresis loops that capture the rate and temperature-dependent stress/strain

history of solder joints during thermal cycling. Stress/strain loops are computed for shear deformations driven by the global CTE mismatch between board and component, and for normal stresses and strains driven by local CTE mismatches between solder and the interconnected parts. The stress/strain analysis follows the exact same procedures that were developed in [4] for SnPb assemblies except that temperature ramp rates are included in the present analysis. Ramp rates are accounted for by performing a step-by-step integration of creep rate equations along the prescribed temperature profile. The methodology was first developed by Hall [5, 6] in the simulation of measured hysteresis loops for SnPb assemblies. The method applies to any shape of a periodic temperature profile, including trapezoidal, saw-tooth and sine profiles. The simplified constitutive model that was selected for SAC387/396 solder includes temperature-dependent elastic and minimum creep rate deformations. The elastic properties (E = E(T) = Young's modulus; G = G(T) = shear modulus; ν = Poisson's ratio) used in the CSE model are based on measurements of SAC specimens at Sandia National Laboratories [7]:

$$E(T) = 2(1+\nu)\, G(T) \quad (2a)$$

$$G(T) = 20.24 - 2.635\ 10^{-2}\ T - 6.503\ 10^{-6}\ T^2 \ \text{GPa} \quad (2b)$$

$$\nu = 0.35 \quad (2c)$$

with the temperature T in degree Celsius. Poisson's ratio had a weak temperature dependence and is given as an average value over the temperature range -55/150ºC [7].

The minimum creep rate equation that is used in the CSE model is in the form of an obstacle-controlled creep model [8] that was fit to tensile creep data [9] in the temperature range -40ºC to 125ºC. The model was shown to apply to surface mount assemblies [8] by predicting the shear strength of SAC Chip Scale Package (CSP) type of joints at temperatures of 25ºC, 75ºC and 125ºC [10]. In tension, the minimum creep rate is given as:

$$\overset{o}{\varepsilon}(/\sec) = 5.0\cdot 10^{-9}\sigma^{5.56}\cdot \exp\left[-\frac{3544}{T(K)}\left(1-\frac{\sigma}{1280}\right)\right] + 6802\sigma^{3.02}\cdot \exp\left[-\frac{11050}{T(K)}\left(1-\frac{\sigma}{181}\right)\right] \quad (3)$$

where the tensile stress σ has units of MPa and the temperature T is in degree Kelvin (K). Assuming that a Von-Mises yield criterion applies, creep rates in shear are:

$$\overset{o}{\gamma}(/\sec) = \sqrt{3}\times \left\{ 5.0\times 10^{-9}\left(\tau\sqrt{3}\right)\sigma^{5.56}\cdot \exp\left[-\frac{3544}{T(K)}\left(1-\frac{\tau\sqrt{3}}{1280}\right)\right] + 6802\left(\tau\sqrt{3}\right)^{3.02}\cdot \exp\left[-\frac{11050}{T(K)}\left(1-\frac{\tau\sqrt{3}}{181}\right)\right] \right\} \quad (4)$$

where the shear stress τ has units of MPa.

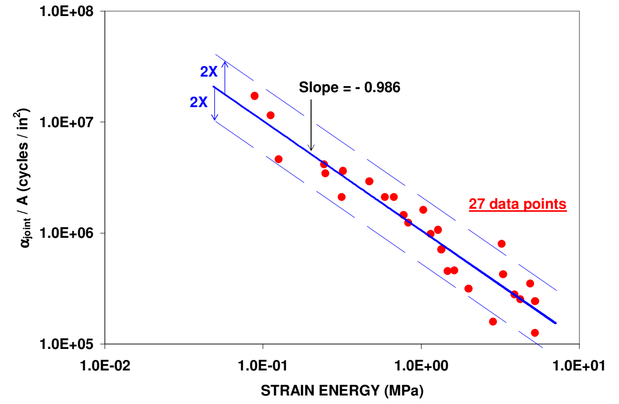

Figure 1: SAC CSE model life / strain energy correlation.

The correlation of SAC387/SAC396 thermal cycling failure data to cyclic strain energy given by the CSE model is as shown in Figure 1. The equation of the best-fit-line through the data points in Figure 1 is:

$$\frac{\alpha_{JOINT}}{A} = \frac{C}{\Delta W^m} \quad (5)$$

where α_{JOINT} is the characteristic life on a per joint basis (using Weibull failure distributions from a population of critical solder joints as opposed to failure distributions for a population of components), A is the solder joint load bearing or crack area, C is a constant, ΔW is the cyclic strain energy density obtained from the area of stress / strain hysteresis loops, and the exponent m is close to 1 (m = 0.986). The 27 data points in Figure 1 cover about two orders of magnitude in each direction and the slope of the centerline correlation is close to -1. The spread of the data around the centerline is a factor of two times, which is typical of fatigue correlations. As discussed in [8], the slope of -1 is consistent with theoretical models and other strain-energy-based empirical correlations for thermal cycling fatigue of soft solders. AFs are thus obtained as the ratio of cyclic strain energies (ΔW) under test and field conditions:

$$AF \equiv \frac{N_f(field)}{N_f(test)} = \frac{\Delta W(test)}{\Delta W(field)} \quad (6)$$

where N_f 's are cycles to failure and ΔW's are cyclic strain energies under test and field conditions. The domain of validity of the CSE model for SAC assemblies is dictated by the lower bound of strain energy values in the empirical correlation in Figure 1. Technically, the model and the ensuing AFs apply to use and test conditions with cyclic strain energies down to 0.1 MPa. In future work, and as more test data becomes available for SAC387/396 assemblies under milder stress conditions, we will check whether the correlation in Figure 1 holds at lower strain energy values.

Finite Element Modeling (FEM)

In addition to the algebraic and CSE model as described above, Finite Element Modeling (FEM) is also utilized in this study for comparison purposes. This represents a natural progression in terms of the capacity of the model to

tackle more complex geometries since FEM models can take into consideration the interaction among components in an assembly with little or no geometric simplification compared to other approaches (For this reason, accurate component construction information is required in order to obtain valid results from the models). It also offers the advantage of being able to solve the full field equations and provide stress/strain information on all solder joints at the end of one model run. However, this approach does require more computational resources as the model complexity increases, particularly with geometric and material non-linearity with temperature dependence.

Three-dimensional (3-D) FEM representation is used in all examples in this paper to ensure proper physics is captured, as opposed to simplified 2-D or slice models that could introduce large percentages of errors. The FEM model basically consists of all the major components and parameters affecting solder joint reliability, such as solder joint diameter, height, solder pad, substrate, printed circuit board, etc. Symmetry condition is taken advantage of whenever appropriate.

As with the CSEM approach, material properties are critical for accurate evaluations of solder joint reliability. As many previous works have shown [11], solder properties derived from bulk specimen are not always reliable for solder interconnects. Thus, it is imperative to use a constitutive equation based on relevant tests. For the three cases in this study, the FEM models use the SAC constitutive equation developed by Subbarayan et al. [12]. The Anand-type of model in [12] was fit to SAC data in both shear and tensile tests in the temperature range 25ºC to 125ºC. Since test data outside this range is not yet available, the creep equation is only valid in the temperature range 25ºC to 125ºC. Consequently, results obtained outside this range should be viewed with caution as discussed in the subsequent sections. For board and package materials, temperature dependent properties are used when measured values are available and reasonable constants are assumed when not.

FEM models are created with the ANSYS software. At the end of each model run, post-processing is performed to check each solder joint to identify areas of high stress or maximum strain energy. In ANSYS, strain energy is given by the output parameter PLWK (Plastic Work). Volumetric averaging of PLWK at the top and bottom interfaces of the solder joints is calculated to obtain the plastic work densities, which can be used to correlate solder damage to cycle life. As in the CSE model, the ratio of the plastic work densities from two temperature cycle profiles yields the acceleration factor.

SCOPE OF AF CASE STUDIES

Case #	**Package Type**	**Conditions**	**Comparison**
1	PBGA	Two test conditions, with test results available.	Model (AM, CSEM, FEM) vs. test AF
2	Ceramic BGA	Three test conditions, with test results available.	Model (AM, CSEM, FEM) vs. two test AFs
3	HiCTE Ceramic FC-BGA	One test condition, two use conditions (main and mini-cycles)	Two AFs predicted by three models (AM, CSEM, FEM)

Table 1: Scope of AF analysis.

The analysis includes the comparison of AFs obtained from the three models and/or test results (see Table 1).

- Case # 1 refers to a Plastic BGA (PBGA) test vehicle and test results from an Industry Working Group (IWG) that conducted an accelerated thermal cycling experiment where the main variable was the dwell time on the hot side of a 0/100ºC test (dwell time = 10 or 60 minutes at 100ºC). The test vehicle and the experiment are as described in [13] with failure distributions as shown in [8].
- Case # 2 is that of a laboratory, ceramic BGA test vehicle subject to two sets of harsh conditions: 0/100ºC and -40/125ºC cycles, and a milder, 30/80ºC cycle. The test vehicle, test conditions and test results are as described in [14].
- Case # 3 is that of a HiCTE ceramic Flip-Chip (FC) BGA subject to main and mini temperature cycles.

In all three cases, a considerable effort went into acquiring geometric details and material properties for package and board materials. For example, in case # 1, the plastic BGA model consists essentially of a multilayer stack material layers: solder mask bottom layer, substrate core, solder mask top layer, die attach, silicon die and overmolding compound, that is a total of 5 or 6 material layers. For each layer, the required modeling input parameters are: layer thickness, glass transition temperature for plastic materials, CTEs (in x- and y- directions, above and below Tg), Young's moduli, and Poisson's ratio. That is, the package model alone requires no less than 5 x 5 = 25 to 6 x 5 = 30 numerical values of input parameters. Material properties are readily available - sometimes under the terms of non-disclosure agreement - from packaging foundries that have an interest in or support board-level reliability studies.

CASE STUDY # 1: PBGA ASSEMBLY

PBGA Models

Overall length dimensions	[mils]	[mm]
Molding Compound Length (at substrate interface)	985.0	25.02
Die Length	667.6	16.96
Die Attach Length (at substrate interface)	686.6	17.44
Substrate Length	1063.0	27.00
Overall thickness dimensions	**[mils]**	**[mm]**
Molding Compound thickness (above die)	30.1	0.76
Die thickness	12.9	0.33
Die Attach thickness	2.8	0.07
Substrate thickness	12.5	0.32
PCB thickness	93.0	2.36
Solder Joint dimensions	**[mils]**	**[mm]**
Solder Joint diameter (at 7 mils from PCB Cu pad)	26.8	0.68
Solder Joint height (Cu pad to Cu pad)	18.8	0.48
Solder Joint Pitch	39.4	1.00
Substrate pad diameter	23.0	0.58
Substrate side solder mask opening	18.0	0.46
PCB pad diameter	15.7	0.40
PCB side solder mask opening	21.5	0.55
Substrate thickness dimensions	**[mils]**	**[mm]**
Solder Mask over Cu (top)	1.2	0.03
Cu	1.0	0.03
Substrate Core	7.9	0.20
Cu	1.0	0.03
Solder Mask over Cu (bottom) - SMD	1.4	0.04
PCB thickness dimensions	**[mils]**	**[mm]**
Solder Mask over Laminate (top) - NSMD	1.8	0.05
NSMD Cu Pad thickness (top layer)	1.8	0.05
Laminate thickness	4.7	0.12
Cu	1.3	0.03
Laminate thickness	21.6	0.55
Cu	1.3	0.03
Laminate thickness	3.7	0.09
Cu	1.4	0.04
Laminate thickness	21.6	0.55
Cu	1.4	0.04
Laminate thickness	3.7	0.09
Cu	1.4	0.04
Laminate thickness	21.6	0.55
Cu	1.3	0.03
Laminate thickness	4.5	0.11
Cu (bottom Cu layer, no solder mask)	1.7	0.04

Table 2: Geometric parameters of PBGA assembly.

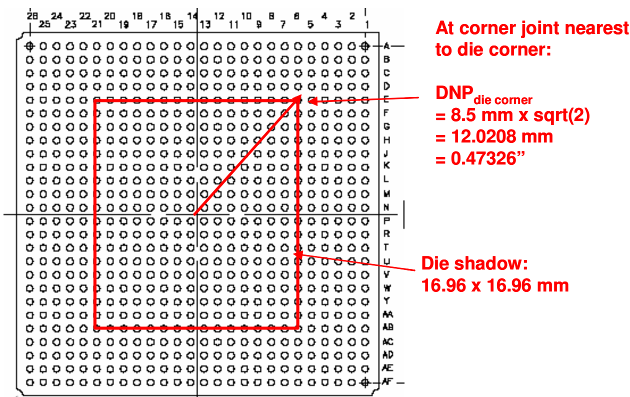

Figure 2: PBGA footprint layout and Distance to Neutral Point (DNP) at joint nearest to die corner.

The 676 I/O PBGA is a 27 x 27 mm package with a 0.33 mm thick, 17 mm x 17 mm die. The test board is 93 mil thick FR-4 with an in-plane CTE of about 13 ppm/C. The raw geometric data that was used to build the PBGA models is as shown in Table 2 (board, package and assembly geometric parameters) and in Figure 2 (footprint layout and maximum DNP at critical joints near the die corners). The purpose of showing these geometric parameters is to illustrate the level of details that is often required to build solder joint reliability models.

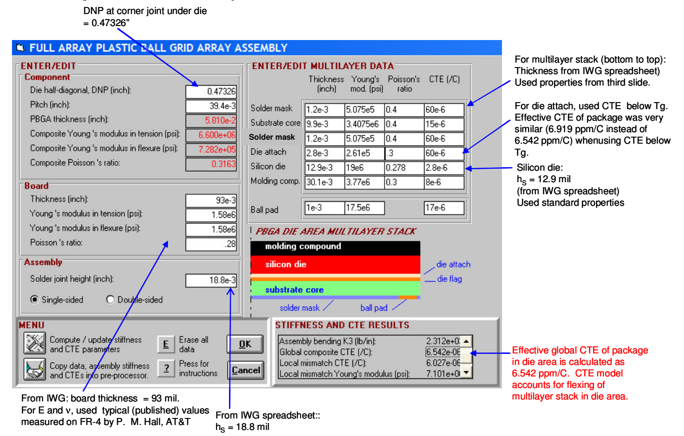

Figure 3: PBGA package and assembly: geometry and material properties that were used to determine assembly stiffness in CSE model.

Figure 3 shows geometric parameters as well as board and package material properties that were used to determine the effective CTE of the package in the die area as well as the assembly stiffness. These parameters are as defined and computed in [4] and are then entered in the CSE program for stress/strain analysis in the SAC PBGA joints near the die corner. Figure 3 further illustrates the level of details that is needed in terms of material properties.

The FEM model of the PBGA test vehicle was built using the exact same raw geometry and material properties as shown above. Figure 4 shows a quarter model of the PBGA676 package with a cross-section exposed.

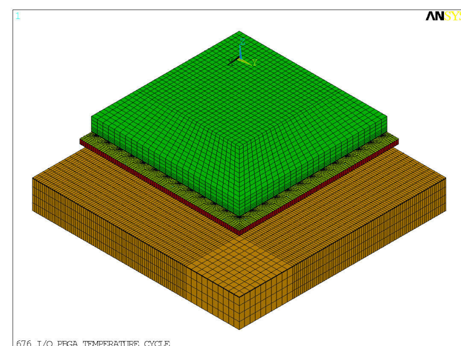

(a)

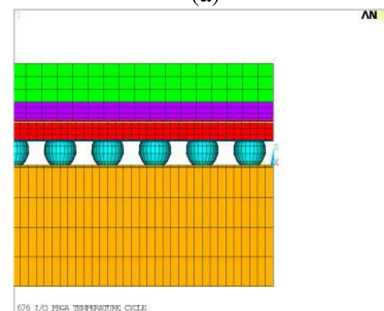

(b)

Figure 4: FEM model: quarter-symmetry model of PBGA assembly (a) and its cross section (b).

The Accelerated Thermal Cycling (ATC) conditions for the PBGA assemblies were thermal cycling between 0ºC and 100ºC with 10 minute ramps, 10 minute dwells at 0ºC, and 10 minutes (“short cycle”) or 60 minutes (“long cycle”) at 100ºC.

PBGA Results And Discussion

FEM Results

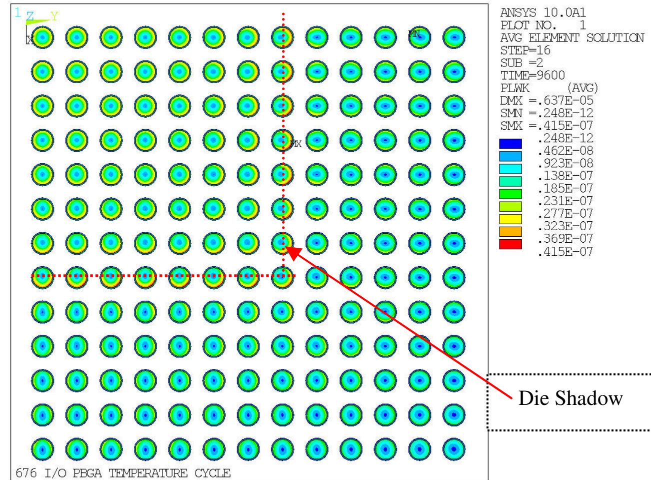

Figure 5: Strain energy contour plots in quarter model of the PBGA SAC assembly.

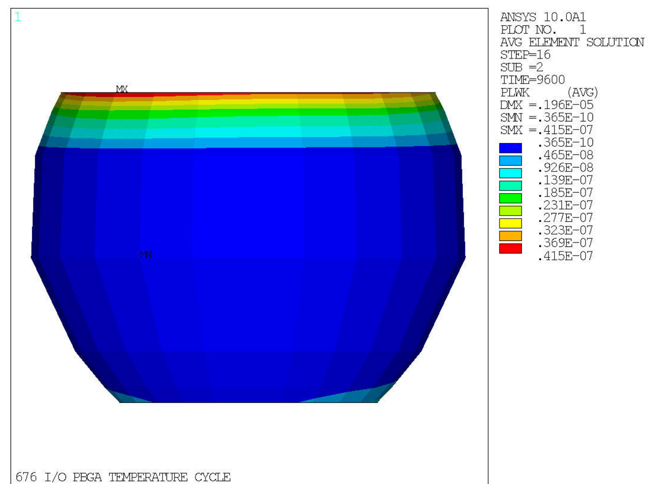

Figure 6: Maximum damage occurs at the PBGA package to solder joint interface (top).

Figure 5 shows the PLWK contour plot of the quarter model (centered at the upper left corner). As can been seen from the plot, the solder joints with the maximum PLWKs are not located at the corner of the solder joint array but in the die shadow area as discovered through dye and pry failure analysis [13]. This is true for both the short and long duration cases (10 minutes vs. 60 minutes at 100ºC). Figure 6 clearly shows that the maximum damage occurs at the package to solder joint interface.

Using the procedure outlined earlier in the Finite Element Modeling section, the acceleration factor between the two profiles is calculated to be AF=1.13. This value compares quite favorably to the Pb-free test case (SnAgCu paste with SnAgCu solder joints, 237°C peak reflow temperature) with the test AF defined as the ratio of the first fails, in which case the test case acceleration factor is AF= (4,390 cycles / 3,424 cycles) = 1.28.

CSEM Results

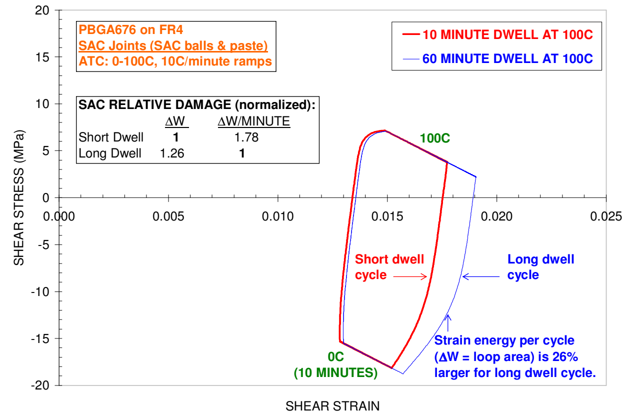

Figure 7: Hysteresis loops of SAC outermost corner joints under die shadow in 676 I/O PBGA on FR-4.

The shear stress / shear strain hysteresis loops for the “short” and “long” dwell cycles are as shown in Figure 7. Further discussion on the amount of stress reduction at the temperature extremes is available in [1]. Based on the ratio of loop areas, the CSE model gives an AF of 1.26.

AM Results

Since the short dwell cycle gives the longest cyclic life in ATC testing, the AF actually is the ratio of cycles-to-failure for “short” to “long” dwell conditions. I.e., in equation (1), subscripts “o” and “t” refer to the “short dwell” and “long dwell” cycles, respectively. With dwell times being the only variable (t_t = 60 minutes, t_o = 10 minutes), the AM model gives:

$$AF \equiv \frac{N_o}{N_t} = \left(\frac{t_t}{t_o}\right)^{0.136} = \left(\frac{60}{10}\right)^{0.136} = 1.276 \qquad (7)$$

Discussion and Comparison to Test AFs

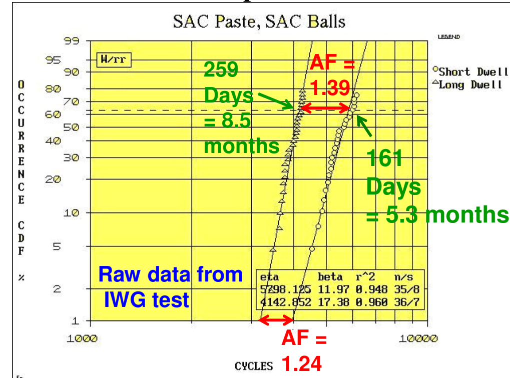

Figure 8: 2P Weibull plot of failure cycles in test for SAC PBGA assemblies subject to ATC (0/100˚C) with short (10 minutes) and long dwell (60 minutes) times at 100˚C.

	AF	AF Calculation Method
TEST	1.24	Calculated as ratio of cycles to 1% failure in test (2P Weibull)
	1.39	Calculated as ratio of cycles to 63.2% failure in test (2P Weibull).
	1.288	Calculated as ratio of failure-free cycles in test (3P Weibull, not shown).
	1.282	Ratio of cycles to first failure
Test Average	1.300	Average of above four AFs in test.

Table 3: Test AFs for SAC PBGA assemblies.

Model	Predicted AF
AM	1.276
CSEM	1.26
FEM	1.13

Table 4: Predicted AFs for SAC PBGA assemblies.

The actual failure distributions and test AFs are shown in Figure 8 and Table 3. The test AFs (Table 3) vary from 1.24 to 1.39 depending on the metric that is used for cycles-to-failure. That is, the test AFs are known with a possible error of about 1.39/1.29 -1 = 12%. For the four metrics used in Table 3, the "average" test AF is 1.3. The predicted AFs - summarized in Table 4 - are in the range 1.13 to 1.276. The three models predict the direction of the dwell time effect correctly and the predicted AFs are all within 15% of the test average (AF = 1.3).

CASE STUDY # 2: CBGA ASSEMBLY UNDER THREE SETS OF TEST CONDITIONS

CBGA Models

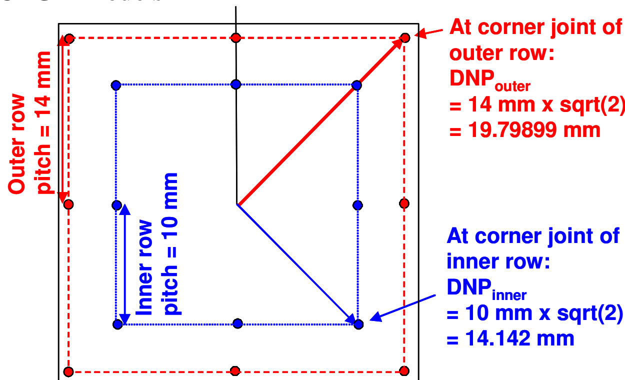

Figure 9: CBGA inner and outer rows of joints.

The second case study is that of a laboratory Ceramic BGA (CBGA) on FR-4, with failure statistics available for three thermal cycling conditions: -40/125ºC, 0/100ºC and 30/80ºC [14]. Construction wise, the CBGA test vehicle is the simplest of the three packages in this paper: a ceramic substrate is attached to a printed circuit board through an inner array of 9 solder joints (3 x 3 full array, 1 mm pitch) at the geometric center of the package and another row of 8 joints at some distance from the center [14]. The 8 solder joints form either an inner or an outer row and are not present together on the same test package. Both rows are shown on the same schematic in Figure 9. Failure times are for either row of joints. Since three temperature profiles are used for the tests, there are altogether 3 x 2 = 6 configurations. The CSE and FE models are run six times to generate six hysteresis loops, one for each configuration of the CBGA assembly with inner or outer row and one for each of the three temperature profiles. The AM model, which does not include geometric parameters, is only run twice to get AFs from the harsher conditions: -40/125ºC and 0/100ºC to the milder condition, 30/80ºC. The models that were built in this study are for the "prototype" test vehicles in [14] since failure statistics were not available for the other "product" test vehicles under milder test conditions in test. Unless indicated otherwise, most geometric details and material properties were available in [14]. The geometric FE model is as illustrated in Figure 10 in the case of the inner row CBGA assembly.

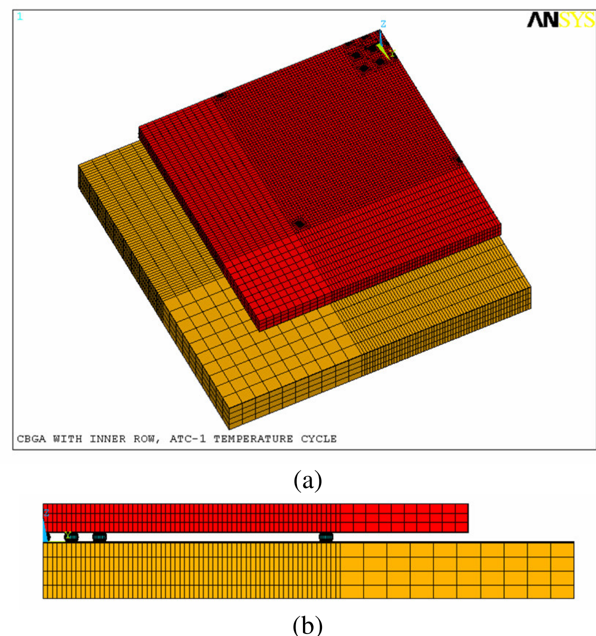

(a)

(b)

Figure 10: FEM model (inner row case): quarter-symmetry model of the CBGA assembly (a) and its cross section (b).

Values of input parameters that were used to build the CSE and FE models are summarized hereafter.

- In the CSE model, the shear stress/strain analysis is set up at outermost corner joint of "Inner" or "Outer" rows with Distance to Neutral Point (DNP) as shown in the package layout in Figure 8.
- The CBGA package is 30 x 30 mm square and 1 mm thick, with a 0.4 mm component pad diameter. The package substrate is "alumina" with the following properties: CTE = 7 ppm/ºC (given in [14]), E = 37e6 psi (assumed standard value), ν = 0.3 (assumed).
- The test board is 2 mm (78.75 mil) thick FR-4. The analysis is done with an assumed board in-plane CTE of 16.5 ppm/C. Note: the corresponding CTE mismatch is 16.5 – 7 = 9.5 ppm/ºC. For a board CTE of 18

ppm/ºC and a more standard CTE of 6.5 ppm/ºC for alumina, the CTE mismatch would be slightly larger at 11.5 ppm/ºC. This should not affect the AF results much since, as shown in [1], AFs have a weak sensitivity to the global CTE mismatch when the latter is large enough. Other assumed properties are typical of standard FR-4 boards: E = 1.58e6 psi (after measurements in [5]), ν = 0.3 (assumed).

- The solder joint height on “proto” test vehicles was given as 0.3 mm (= 11.811 mil). In the CSE model, the solder joint load bearing or crack area is 1.94779 in^2 based on a 0.4 mm (15.748 mil) solderable pad diameter on component side.
- Measured temperature profiles (Figure 3 in [14]) have a cycle length of about 80 minutes. Estimated dwell times and linearized ramps entered in the CSE and FE models are as shown in Figure 11.

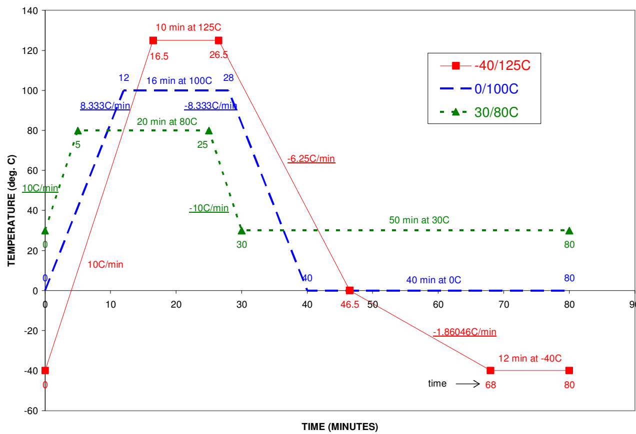

Figure 11: Temperature profiles used in CSE & FE models.

CBGA Results

FEM Results

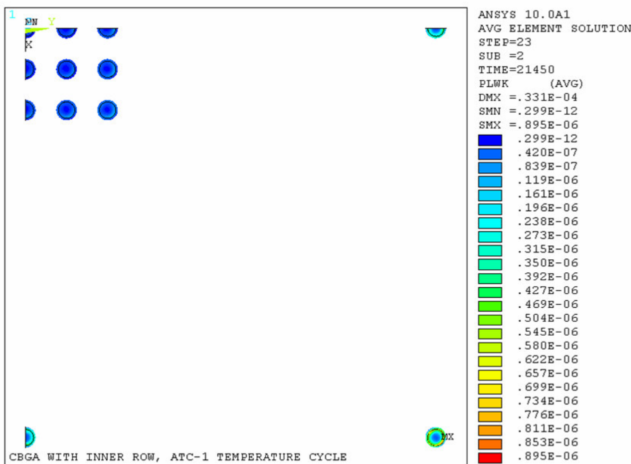

Figure 12: Strain energy contour plots in quarter model of the CBGA (inner row) SAC assembly.

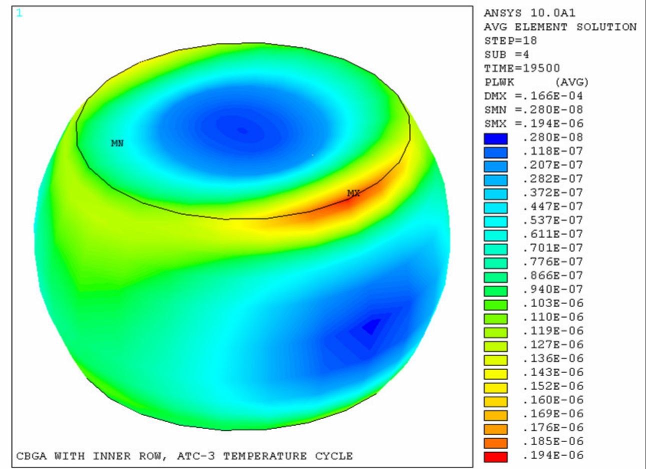

Figure 13: Maximum damage occurs at the CBGA package to SAC solder joint interface (top).

Strain energy contour plots are shown in Figures 12 and 13 in the case of the “inner” row CBGA assemblies. Similar patterns were obtained in the case of the “outer” row CBGA assemblies. As seen in Figure 12, the maximum strain energy is at the outermost corner joints and energy values in the inner array of joints near the center of the package are much lower. i.e., the inner array of joints carries very little stress. Strain energy in the outermost corner joints is the highest at the joint to package interface (Figure 13) and, as expected, the maximum strain energy is at the edge of the solder joint to package interface the furthest away from the neutral axis of the CBGA.

ATC Condition	Inner Row Assembly	Outer Row Assembly
-40/125ºC	5.44	5.82
0/100ºC	2.74	2.89

Table 5: Calculated AFs from FEM strain energy results.

Calculated AFs to extrapolate from the harsher conditions to the milder cycle (30/80ºC) are given in Table 5. The FEM AFs show a weak dependence on the row size with the AFs being 5.5% and 7% larger for the outer row assemblies than for the inner row assemblies in the case of 0/100ºC and -40/125ºC ATC profiles, respectively. As mentioned previously, the creep equation is not applicable for temperatures below 25ºC but is used nevertheless for comparison purposes.

CSE Results

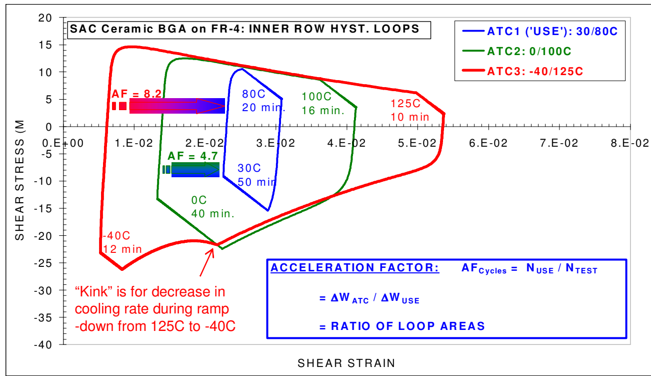

(a) Inner row assembly.

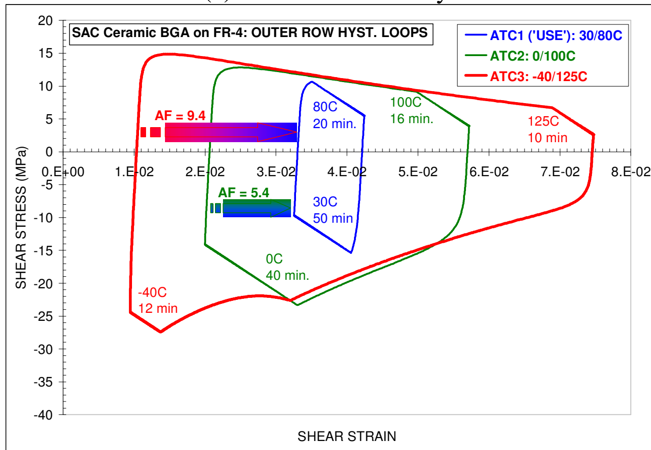

(b) Outer row assembly.

Figure 14: CBGA shear stress/strain hysteresis loops.

The shear stress / shear strain hysteresis loops at the outermost corner joints of the inner and outer row CBGA assemblies are shown in Figure 14. The shown AFs were obtained as ratios of loop areas. The strain energy values for all loops were within the range of the empirical correlation of SAC thermal cycling data in Figure 1. AFs are calculated for extrapolation of failure cycles from -40/125ºC (ATC3 condition) and 0/100ºC (ATC2) to the milder condition 30/80ºC (ATC1). The calculated AFs suggest a slight row size dependence since the AFs for the outer row assemblies are about 15% larger than for the inner row assemblies. This is less than the difference in maximum DNPs (see Figure 9) since the DNP of the outer row corner joints is 40% larger than that of the inner row corner joints.

AM Results

EXAMPLE: Ceramic "BGA" prototype after Salmela et al., SMTA Journal, Vol. 18, No. 2, 2005, pp. 15-21; conditions: ATC3 = -40/125C and ATC1 = 30/80C

AF is defined as: N(30/80C) / N(-40/125C),
thus: "30/80C" = "o" condition and "-40/125C"= "t" condition

	"t" condition -40/125C = "ATC3"	"o" condition 30/80C = "ATC1"	AF		
Tmax (deg.C)	125	80	term 3:	2.01	Arrhenius term
Tmin (deg. C)	-40	30			
Dwell (min.)	10	20	term 2:	0.91	Dwell time factor
ΔT (deg. C)	165	50	term 1:	23.66	Delta T factor
		AF_Predicted = term3 x term2 x term1		43.36	

(a) -40/125ºC to 30/80ºC

EXAMPLE: Ceramic "BGA" prototype after Salmela et al., SMTA Journal, Vol. 18, No. 2, 2005, pp. 15-21; conditions: ATC2 = 0/100C and ATC1 = 30/80C

AF is defined as: N(30/80C) / N(0/100C),
thus: "30/80C" = "o" condition and "0/100C"= "t" condition

	"t" condition 0/100C = "ATC2"	"o" condition 30/80C = "ATC1"	AF		
Tmax (deg.C)	100	80	term 3:	1.39	Arrhenius term
Tmin (deg. C)	0	30			
Dwell (min.)	16	20	term 2:	0.97	Dwell time factor
ΔT (deg. C)	100	50	term 1:	6.28	Delta T factor
		AF_Predicted = term3 x term2 x term1		8.49	

(b) 0/100ºC to 30/80ºC

Table 6: CBGA AF calculations as per equation (1).

The calculation of algebraic AFs for the CBGA assemblies is as shown in Tables 6a and b with the contribution of each factor in equation (1) being highlighted. The temperature swing (ΔT) factor ("term 1") appears to contribute the most to the composite AFs.

Discussion and Comparison of Test and Model AFs

AF COMPARISONS: OUTER ROW CBGA ASSEMBLIES

DATA SOURCE	AF = N(30/80C) / N(-40/125C)	RATIO = MODEL AF / TEST AF
TEST: N63% RESULTS (AF = 241/18)	13.39	1
MODEL:		
FEM	5.82	0.43
CSEM	9.4	0.70
AM	43.36	3.24

(a) Outer Row AFs

AF COMPARISONS: INNER ROW CBGA ASSEMBLIES

DATA SOURCE	AF = N(30/80C) / N(-40/125C)	RATIO = MODEL AF / TEST AF
TEST: N63% RESULTS (AF = 430/43)	10.00	1
MODEL:		
FEM	5.44	0.54
CSEM	8.2	0.82
AM	43.36	4.34

(b) Inner Row AFs

Table 7: Acceleration factors from -40/125ºC to 30/80ºC.

AF COMPARISONS: OUTER ROW CBGA ASSEMBLIES

DATA SOURCE	AF = N(30/80C) / N(0/100C)	RATIO = MODEL AF / TEST AF
TEST: N63% RESULTS (AF = 241/58)	4.16	1
MODEL:		
FEM	2.89	0.70
CSEM	5.4	1.30
AM	8.49	2.04

(a) Outer Row AFs

AF COMPARISONS: INNER ROW CBGA ASSEMBLIES

DATA SOURCE	AF = N(30/80C) / N(0/100C)	RATIO = MODEL AF / TEST AF
TEST: N63% RESULTS (AF = 430/117)	3.68	1
MODEL:		
FEM	2.74	0.75
CSEM	4.7	1.28
AM	8.49	2.31

(b) Inner Row AFs

Table 8: Acceleration factors from 0/100ºC to 30/80ºC.

AFs from test and modeling are given in Tables 7 and 8 going from -40/125°C and 0/100ºC, respectively, to 30/80ºC conditions. For each of the two harsh conditions, AFs are also given for "inner" and "outer" row assemblies. A few observations are worth highlighting, based on the AFs in Tables 7 and 8:

- Test AFs are based on characteristic lives from Table 1 in [14]. First failures and statistical distributions were not available, so we do not have a sense of how wide confidence bands were and we cannot estimate error margins on the experimental AFs.

- The FEM approach appears to be on the conservative since it predicts AF values within -25 to -30% (0/100ºC test) or -46 to -57% (-40/125ºC test) of the experimental AFs. However, AFs predictions within +/-30% of experimental results are thought to be reasonable, in general, given possible experimental errors, the statistical distribution of failure times and the width of confidence bands on failure distributions. The larger error for the FEM-predicted AF with -40/125ºC test conditions is perhaps due to the fact that the constitutive model used in the FEM approach is based on SAC mechanical data above room temperature. This will be investigated in future work by using an appropriate constitutive model that covers a wider temperature range.

- For both test conditions (-40/125ºC and 0/100ºC) the CSEM approach predicts AFs within +/-30%.

- The AM approach overpredicts the CBGA AFs by about three to four times for the -40/125ºC test. As discussed in [2], the Norris-Landzberg type of model with the initial set of constants given in equation (1) should not be used for cycles with very cold temperatures. However, it is not clear why the model overpredicts the AF by about 2 times for the 0/100ºC test.

- In test, the DNP effect (outer row vs. inner row assemblies) on AFs is a factor of 13.39 / 10 = 1.339 time under -40/125ºC test conditions. The DNP effect is 4.16 / 3.68 = 1.13 times under 0/100ºC test conditions. The DNP effect on AFs is not negligible (an effect of 13 to 34%). In comparison:

    - The FEM approach gives a DNP effect on AFs of 5.82 / 5.44 = 1.07 times under -40/125C conditions, and 2.89 / 2.74 = 1.05 times under 0/100C test conditions.
    - The CSEM approach gives a DNP effect of about 1.15 times under both test conditions: 9.4 / 8.2 = 1.146 times for the -40/125ºC test and 5.4 / 4.7 = 1.149 for the 0/100ºC.
    - The AM model does not include a DNP factor.

CASE STUDY # 3: FLIP-CHIP BGA

Flip-Chip BGA Model

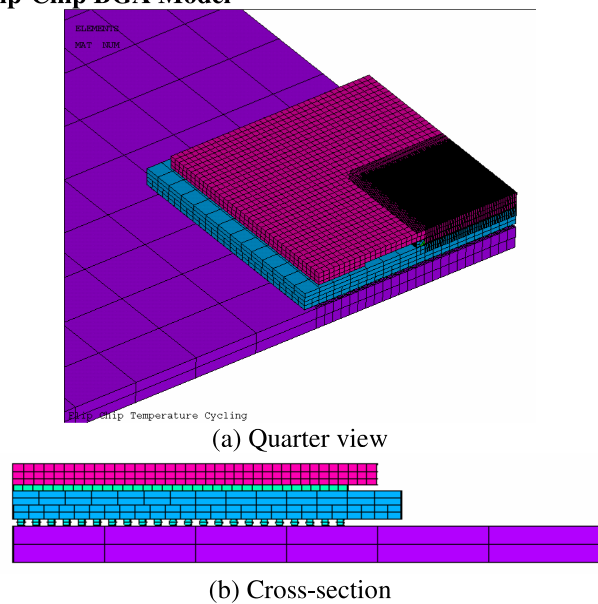

(a) Quarter view

(b) Cross-section

Figure 15: FE model of FC-BGA assembly.

A flip chip package with a lid (or heat spreader) is attached to a printed circuit board with a full 43 x 43 array, 1 mm pitch SAC solder joints. The FE model (Figure 15) of the package includes the major elements of the construction: die, underfill, thermal grease and heat-spreader. Since the package substrate is rather thick and rigid (hi-CTE ceramic), and the thermal grease is compliant, the CSE analysis is simplified by reducing the model to that of the ceramic substrate working alone against the FR-4 board. I. e., the CSE model does not include the die and package lid. Further geometric details and material properties are not listed for the sake of brevity.

The goal of this case study was to determine AFs to extrapolate ATC test results (0/100ºC, 10 min. ramps, 10 minute dwells) to use conditions that include a main temperature cycle (~ 25C to 85ºC) and mini-temperature cycles (~ 75C to 85ºC) that arise due to product usage. Details of the temperature profiles are shown in Figure 16 to illustrate rapid changes in ramp rates. The thermal stress/strain analysis in both the CSE and FE models followed the exact temperature profiles shown in Figure 16. AFs were determined to compare the predictions of the three models (AM, CSEM and FEM) for use conditions with quite different temperature swings: ΔT ~ 60ºC for the main cycle, and ΔT ~ 10ºC for the mini-cycles.

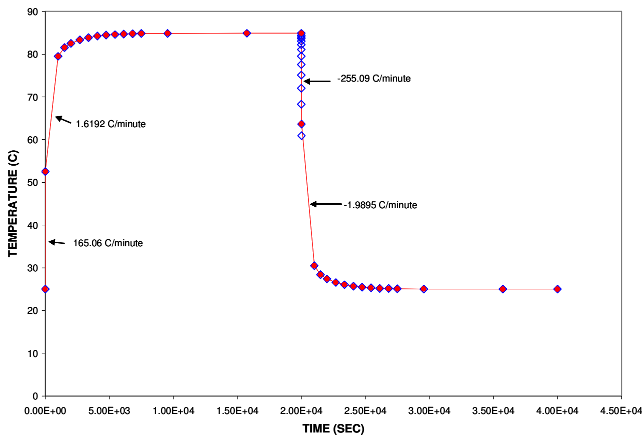

(a) Main temperature cycle: "25/85ºC"

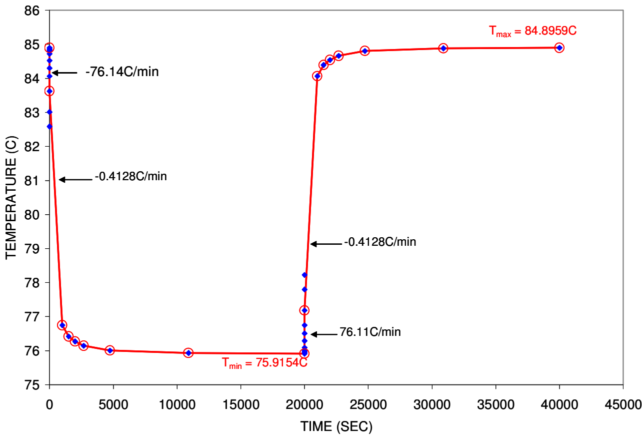

(b) Mini-cycle temperature profile: "75/85ºC"

Figure 16: Use temperature profiles.

Stress/Strain Analysis and AM Results

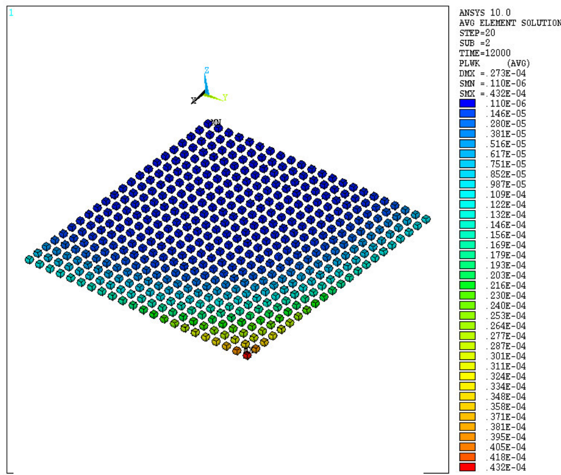

Figure 17: FC-BGA strain energy contours.

FEM strain energy contours in Figure 17 show that, as expected, the most damage occurs at the outermost corner joints.

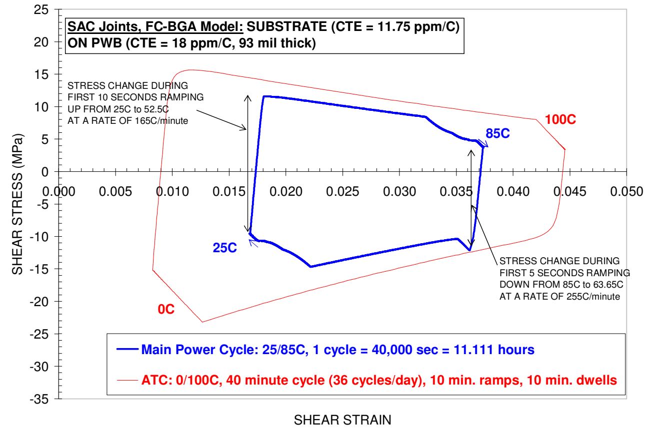

(a) ATC and Main Temperature Cycle

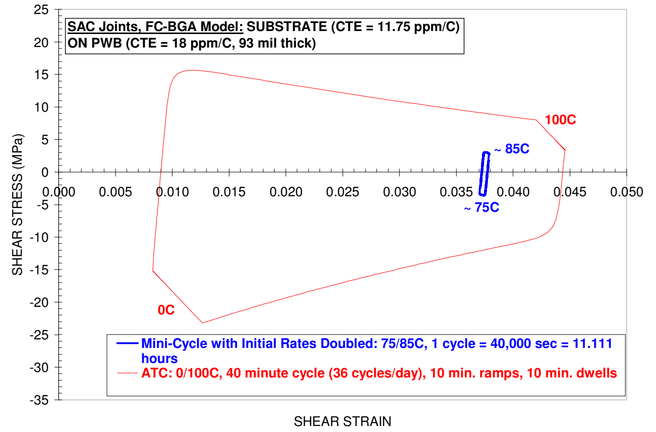

(b) ATC and Mini-Temperature Cycle

Figure 18: CSE FC-BGA model hysteresis loops.

Figure 18 shows the global CTE mismatch hysteresis loops at the outermost corner joints of the FC-BGA assembly under ATC, main and mini-cycle conditions. The local CTE mismatch hysteresis loops are not shown but it was found that they contributed a very small percentage to the total cyclic strain energy for the three thermal profiles. The mini-cycle loop in Figure 18b is considerably smaller than the other two loops, which could potentially lead to large errors in predicted AFs for mini-cycle conditions. This was one of the motivating factors to compare predicted AFs obtained from several models.

Main-Cycle AF Calculations					
	USE	TEST		AF	
Tmax (deg.C)	85	100	term 3:	1.28	= Arrhenius term
Tmin (deg.C)	25	0			
Dwell (min.)	228 (~ 3.8 hours)	10	term 2:	0.65	= dwell time factor
DT	60	100	term1:	3.87	= ΔT factor
	AF_Predicted = term1 x term2 x term3			3.23	

(a) ATC to main cycle: ~ 25/85ºC

Mini-Cycle AF Calculations					
	USE	TEST		AF	
Tmax (deg.C)	84.8959	100	term 3:	1.28	= Arrhenius term
Tmin (deg.C)	75.9154	0			
Dwell (min.)	308.3	10	term 2:	0.63	= dwell time factor
	(~ 5.14 hours)				
ΔT	8.9805	100	term1:	593.96	= ΔT factor
AF_Predicted = term1 x term2 x term3				477.11	

(b) ATC to mini-cycle: ~ 75/85ºC

Table 9: AF calculations based on AM model

AF calculations using the AM model are as shown in Tables 9a and b for main and mini-cycle use conditions, respectively. Again, temperature swings (first term in equation 1) have a dominant weight in the final AF results.

AF Summary And Discussion

MAIN TEMPERATURE CYCLE: AF COMPARISONS		
MODEL	AF	AF Ratio = AM Model/ Other AF
AM	3.23	1
FEM	2.23	1.448
CSEM	2.345	1.377

(a) Main cycle: ~ 25/85ºC

MINI-TEMPERATURE CYCLE: AF COMPARISONS		
MODEL	AF	AF Ratio = AM Model/ Other AF
AM	477.11	1
FEM	322.47	1.480
CSEM	300.004	1.590

(b) Mini-cycles: ~ 75/85ºC.

Table 10: FC-BGA AF comparison for three models.

AFs from the three models are summarized in Table 10.

- As expected, the AFs for mini-cycles are much larger than for the main cycles, by over two orders of magnitude.
- The AFs from strain-energy based models are in very close agreement. For main and mini- cycles, the FEM and CSEM AFs are within 5% and 7.5% of each other, respectively. This is quite remarkable given the differences in selected creep laws as well as differences in stress/strain analysis techniques. The agreement also holds for both small and large temperature swings.
- The AFs predicted by the AM approach are 37% to 59% larger than AFs from the FEM and CSEM approaches.

CONCLUSIONS

In this paper, three package assemblies were analyzed to determine acceleration factors (AFs) for Pb-free SAC (SnAgCu) assemblies using Algebraic Model (AM), Compact Strain Energy Model (CSEM) and Finite Element Model (FEM) approaches. Except for the PBGA case, the AM approach tends to predict higher AFs, which could overestimate solder joint fatigue performance and lead to weak designs that may not survive field conditions. Caution must be exercised when using the AM approach beyond its domain of validity.

On the other hand, the CSEM and FEM approaches predict AFs more in line with test data. This should not come as a surprise since both approaches are based on strain energy accumulation in the solder joints, which is known as the driving force for solder damage. Moreover, both approaches take geometry and material properties into consideration, which cannot be accounted for in the AM approach. The package dependence of AFs is well established for SnPb assemblies [15]. Based on the observed and predicted effect of maximum DNPs on SAC AFs in case study # 2 in this paper, the AF package dependence appears to hold as well for SAC assemblies.

One point worth noting is that the FEM models in this paper tend to yield more conservative AFs. This should be viewed as an exception rather than the rule since the FEM results depend on the creep equation that is used for SAC solders. As discussed previously, the particular creep equation that was used in this paper was based on test data from 25ºC to 125ºC, which does not cover temperatures below ambient. In future work, another equation that is valid in the temperature range -40ºC to 125ºC will be utilized.

AFs play a critical role in the assessment of Pb-free product solder joint reliability. AF modeling of SAC assemblies is as much in the infancy stage as Pb-free technology itself and considerable efforts are needed to validate AF predictions and estimate their accuracy. Based on examples given in this paper, and other on-going investigations, an error margin of about 30% on AFs appears as a reasonable and feasible goal. Last, given possibly large differences in predicted AFs from different models, it is worthwhile to exercise several approaches to better gauge the accuracy of AF results.

ACKNOWLEDGMENT

The authors wish to thank Keith Newman, Sun Microsystems, for his valuable input and insightful discussions in the PBGA and FC-BGA case studies. Our appreciation also goes to Gregory Henshall at HP for his probing questions and constructive critiques, which has resulted in better clarity in the presentation.

REFERENCES

1. Clech, J-P., "Acceleration factors and thermal cycling test efficiency for lead-free Sn-Ag-Cu assemblies", Proceedings, SMTA International Conference, Chicago, IL, Sept. 25-29, 2005, pp. 902-917.
2. Pan, N., Henshall, G. A., Billaut, F., Dai, S., Strum, M. J., Benedetto, E. and Rayner, J. “An Acceleration Model for Sn-Ag-Cu Solder Joint Reliability Under Various Thermal Cycle Conditions”, Proceedings, SMTA International Conference, Chicago, IL, September 25-29, 2005.
3. Norris, K. C. and A. H. Landzberg, A. H, "Reliability of Controlled Collapse Interconnections," *IBM Journal of Research and Development*, May 1969, pp. 266-271.
4. Clech, J-P., "Solder Reliability Solutions: a PC-based design-for-reliability tool", Proceedings, Surface Mount International Conference, Sept. 8-12, 1996, San Jose,

CA, pp. 136-151. Republished in *Soldering and Surface Mount Technology*, Wela Publications, British Isles, Vol. 9, No. 2, July 1997, pp. 45-54.

5. Hall, P.M., “Forces, moments, and displacements during thermal chamber cycling of leadless ceramic chip carriers soldered to printed boards”, *IEEE Transactions on Components, Hybrids and Manufacturing Technology,* 1984, Vol. 7, No. 4, Dec. 1984, pp. 314-327.
6. Hall, P. M., “Creep and stress relaxation in solder joints of surface mounted chip carriers”, *IEEE Transactions on Components, Hybrids and Manufacturing Technology*, 1987, Vol. CHMT-12, No. 4, Dec. 1987, pp. 556-565.
7. Vianco, P. T., Rejent, J. A. and Kilgo, A. C., “Time-independent mechanical and physical properties of the ternary 95.5Sn-3.9Ag-0.6Cu Solder”, *Journal of Electronic Materials*, Vol.32, No. 2, 2003, pp. 142-151.
8. Clech, J-P., "An obstacle-controlled creep model for Sn-Pb and Sn-based lead-free solders", Proceedings, SMTA International Conference, Chicago, IL, September 26-28, 2004.
9. Pang, J. H. L., Xiong, B. S. and Low, T. H., “Creep and fatigue characterization of lead free 95.5Sn-3.8Ag-0.7Cu”, Proceedings, 54th Electronic Components and Technology Conference, Las Vegas, NV, June 1-4, 2004, pp. 1333-1337.
10. Pang, J. H. L., Xiong, B. S., Neo, C. C., Zhang, X. R. and Low, T. H., “Bulk solder and solder joint properties for lead-free 95.5Sn-3.8Ag-0.7Cu solder alloy”, Proceedings, IEEE 53rd Electronic Components and Technology Conference, New-Orleans, LA, May 27-30, 2003.
11. Bhate, D., Chan, D., Subbarayan, G. and Chiu, T.C., “Solder interconnection specimen design and test control procedure for valid constitutive modeling of solder alloys”, IEEE Intersociety Conference on Thermal and Thermomechanical Phenomena in Electronic Systems, San Diego, CA, May 31-Jun 1, 2006.
12. Subbarayan, G. et al., Texas Instruments Internal Report, 2005.
13. Bath, J., Sethuraman, S., Zhou, X., Willie, D., Hyland, K., Newman, K., Hu, L., Love, D., Reynolds, H., Koichi, K., Chiang, D., Chin, V., Teng, S., Ahmed, M., Henshall, G., Schroeder, V., Lau, J., Nguyen, Q., Maheswari, A., Cannis, J., Clech, J.-P. and Gibson, C., “Reliability evaluation of lead-free SnAgCu PBGA676 components using tin-lead and lead-free SnAgCu solder paste”, Proceedings, SMTA International Conference, Chicago, IL, September 25-29, 2005.
14. Salmela, O., Andersson, K., Särkkä, J.and Tammenmaa, M., “Reliability analysis of some ceramic lead-free solder attachments”, 2005 Proceedings, Pan Pacific Microelectronics Symposium, SMTA, January 25-27, 2005, Kauai, Hawaii, pp. 161-169. Also in *Journal of Surface Mount Technology*, SMTA, Vol. 18, Issue 2, April-June 2005, pp. 15-21.
15. Sastry, V. S., Manock, J. C. and Ejim, T. I., "Effect of thermal cycling ramp rates on solder joint fatigue life", Proceedings, SMTA International Conference, Rosemont, IL, September 24-28, 2000, pp. 331-336. Also in *Journal of Surface Mount Technology*, January 2001, Vol. 14, Issue 1, pp. 23-28.